

Pattern Formation and Flocking for Particles Near The Jamming Transition on Resource Gradient Substrates

L. Varga¹, A. Libál¹, C. Reichhardt², and C. J. O. Reichhardt²

¹ *Mathematics and Computer Science Department,
Babeş-Bolyai University, Cluj-Napoca 400084, Romania*

² *Theoretical Division and Center for Nonlinear Studies,
Los Alamos National Laboratory, Los Alamos, New Mexico 87545, USA*

(Dated: July 8, 2022)

We numerically examine a bidisperse system of active and passive particles coupled to a resource substrate. The active particles deplete the resource at a fixed rate and move toward regions with higher resources, while all of the particles interact sterically with each other. We show that at high densities, this system exhibits a rich variety of pattern forming phases along with directed motion or flocking as a function of the relative rates of resource absorption and consumption as well as the active to passive particle ratio. These include partial phase separation into rivers of active particles flowing through passive clusters, strongly phase separated states where the active particles induce crystallization of the passive particles, mixed jammed states, and fluctuating mixed fluid phases. For higher resource recovery rates, we demonstrate that the active particles can undergo motility induced phase separation, while at high densities, there can be a coherent flock containing only active particles or a solid mixture of active and passive particles. The directed flocking motion typically shows a transient in which the flow switches among different directions before settling into one direction, and there is a critical density below which flocking does not occur. We map out the different phases as function of system density, resource absorption and recovery rates, and the ratio of active to passive particles.

I. INTRODUCTION

There is a large class of particle-like systems that can exhibit collective motion when coupled to a substrate. In some cases, the motion is the result of driving by an external bias, such as vortices in type-II superconductors driven over random landscapes [1, 2], moving charged colloidal particles interacting with a rough landscape [3–5], frictional systems [6], and the larger class of systems that exhibit collective depinning phenomena [7, 8]. As a function of increasing external bias or changing particle density, these systems exhibit distinct types of flow patterns. In elastic flow, all of the particles travel at the same speed and keep the same neighbors, while in plastic flow, the motion is broken into rivers or channels of flow where portions of the system are pinned while other portions are mobile [7, 8]. Often, transitions appear between different flow states as a function of driving, such as the dynamical ordering of a plastically moving phase into a moving crystal or moving smectic phase [8–10]. In bidisperse particle assemblies where each particle species has a different coupling to the external biasing or the substrate, mixed flow or fully phase separated states can appear. An example of this is the laning transition studied for bidisperse particles moving in opposite directions [11, 12], where possible dynamic phases include spatially separated lanes as well as mixed flowing or jammed configurations [13].

Active matter or self-propelled particles represent another system that can exhibit collective dynamic phases [14, 15], such as fluid states, directed motion, and motility induced phase separated states in which an active solid coexists with a low density active fluid [16–21]. In

the presence of a substrate, additional phases appear, including aligned lanes or plastically moving states with co-existing regions of moving and immobile particles [22]. In flocking systems represented by the Vicsek model [23, 24], the particles form flocks that move in a fixed direction at constant velocity. In many flocking systems, there is a critical density at which a transition occurs from a fluid state into a coherently moving state.

More recently, another type of active matter system was introduced in which the motion of the particles is produced via feedback from a resource substrate [25]. This model was initially proposed for robot swarms on resource landscapes that are intended to mimic the motions of foragers. The robots or moving particles deplete the resources at a certain rate and the resources recover at a different rate. The particles are subjected to a force termed a field drive that moves them toward regions with larger resource concentrations [25]. This system shows a series of dynamic phases including liquid, crystalline, and jammed states as the resource consumption and replenishment rates are varied. A modification of this model was used to study the addition of evolutionary rules to the robots [26]. A different variation of this model employed particles coupled to an array of substrate sites that each have a resource parameter [27]. Any particle that covers a site absorbs the resources at a rate r_{abs} , while at the same time, the sites recover the resources at another rate r_{rec} up to a maximum resource level. A two-dimensional realization of this model was explored for interacting disks at an area coverage or density of $\phi = 0.549$, well below the jamming density of $\phi = 0.9$ expected for monodisperse disks [28]. At these lower densities, distinct phases appear, including

a liquid-like continuously fluctuating phase when the resource absorption and recovery rates are similar and a frozen phase when the recovery rate is so high that the resource gradient vanishes and the particles experience no driving force. At low recovery rates, pulsating motion arises that is similar to the patterns found in excitable media [29]. The pulsating waves form when the resources must build up over time, so that when the resource gradient becomes large enough, the particles move in a front. This causes the resource levels to drop, and the particles remain frozen again until the resources are sufficiently replenished to generate the next wave. The effect of adding passive particles, which interact only with other particles but not with the substrate, was also considered. For high resource recovery rates, the active particles can push the passive particles together into a high density crystalline passive phase surrounded by a lower density fluid of active particles and a small number of passive particles. This phase separation resembles the motility induced phase separation observed in active matter systems [16–21], except it occurs for the passive particles.

In this work we study the high density limit of the resource landscape model introduced in Ref. [27], and consider the jamming of active and passive particle mixtures as well as systems containing only active particles. We concentrate on three regimes. In the scarce regime, the resource absorption rate is high and the recovery rate is low; in the balanced regime, the absorption rate is about four times higher than the recovery rate; and in the plentiful regime, the recovery rate and absorption rates are nearly equal. In the scarce regime, we find two types of phase separated states including a partial clustering regime and a river-like regime where the active particles move in winding paths between islands of passive particles. At the highest densities, a mixed jammed state can form. In the balanced regime, we find strong phase separation when the active particles push the passive particles into dense crystalline arrangements with cluster, stripe, void and uniform morphologies similar to those found in equilibrium phase separating systems [30–33]. The active particles themselves can also form crystalline motility induced phase separated clusters where the activity induces the self-clustering. At high densities, the clusters undergo switching directed motion in which flow persists in one direction for a period of time before switching to a new direction, and at even higher densities, a flocking state appears where clusters containing a mixture of active and passive particles continuously move in a fixed direction, similar to what is observed in the Vicsek model [23, 24]. Within the balanced regime, flocking can only occur in the presence of passive particles, which are necessary to produce asymmetric resource gradients in the substrate. In the plentiful regime, flocking is possible even if all of the particles are active, and there is also a phase where the active particles flock while the passive particles form a stationary crystalline solid. We find that the velocity of the directed motion is non-monotonic as a function of recovery rate, starting at a low value for

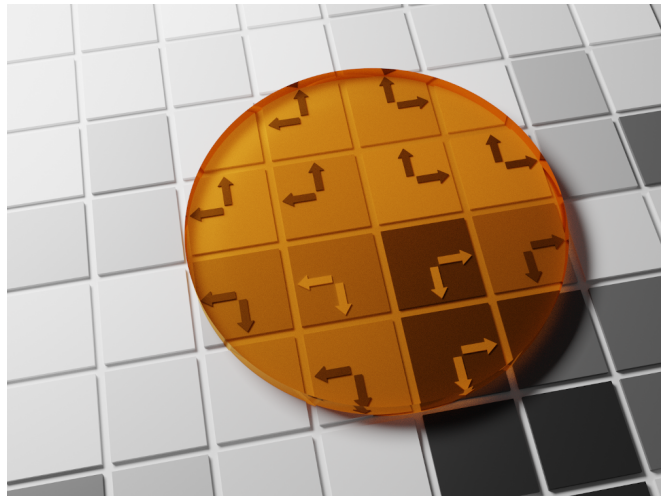


FIG. 1. Schematic illustration of the interaction of an active particle (orange disk) with the resource substrate (boxes). The resource sites may have high (white) or low (black) levels of resource S_g at any given time step. Each particle occludes 12 grid sites in a cross geometry, indicated by the boxes containing arrows. To represent a resource gradient-induced drive, an occluded grid site i exerts a force on the particle in the direction of each arrow with a magnitude proportional to S_g^i . If the resource concentration is flat in any direction, the particle will experience no net force in that direction. The active particle depletes the resource in each of the 12 grid sites at a rate r_{abs} , while all of the grid sites recover resources at a rate r_{rec} up to a maximum level of $S_g^i = 1$.

low recovery rates and increasing with increasing recovery rate, but dropping back to a value close to zero at higher recovery rates when the resource gradients become very weak or are absent.

II. SIMULATION

We simulate a system containing an active substrate of size $L_x \times L_y = 100 \times 200$ that is covered by a grid of 200×400 square cells of size $l_g \times l_g$, where $l_g = 0.5$. Each grid cell i has a resource value S_g^i that can change continuously between $S_g^i = 0$ and $S_g^i = 1$. An assembly of N disk-like particles with radius $R = 1.0$ is placed on the sample, which has periodic boundary conditions in the x and y directions. Particles denoted as active couple to the substrate and interact sterically with other particles, while passive particles do not couple to the substrate and experience only steric particle-particle interactions. During each time step, there is a recovery and absorption stage and a movement stage, in that order.

In the recovery and absorption stage, each active particle interacts with the 12 cells closest to it on the underlying grid, which form a 4×4 cross-like pattern with the corner cells missing, as illustrated in Fig. 1. The center of the particle is above one of the four central grid cells in this pattern. The amount of resource S_g^i

at cell i is first subjected to recovery, and is then absorbed if the cell is occluded by an active particle. The overall equation describing the resource level evolution is $S_g^i(t + \Delta t) = S_g^i(t) + r_{\text{rec}} - O_g^i r_{\text{abs}}$ where $S_g^i(t)$ is the amount of resource in cell i at the beginning of the recovery stage, r_{rec} is the resource recovery rate, r_{abs} is the resource absorption rate by the active particle, $O_g^i = 1(0)$ if the grid site is occluded (unoccupied), and a factor of the simulation time step $\Delta t = 0.005$ has been folded in to the definitions of r_{rec} and r_{abs} . Due to the fact that the value of S_g^i is bounded within the range $0 \leq S_g^i \leq 1$, in our actual implementation the recovery of the resource cells is computed separately from the absorption, with recovery calculated first followed by calculation of absorption. Recovery occurs regardless of whether the cell is occluded by an active particle, and it is subject to the constraint that the resource level of any cell cannot go above $S_g^i = 1$. Cells that are occluded by an active particle then experience an absorption step subject to the constraint that the amount of resource S_g^i at a cell is not allowed to drop below $S_g^i = 0$. Cells that are not occluded by an active particle experience no absorption.

In the movement stage, particle-particle interaction forces are computed and added to the driving force from the grid on the active particles, giving an overdamped equation of motion of

$$\eta \mathbf{v}_i = \mathbf{F}_i^g + \mathbf{F}_i^{pp} \quad (1)$$

for particle i , where $\mathbf{v}_i = d\mathbf{r}_i/dt$ is the velocity of the particle and $\eta = 1$ is the damping constant. An occluded cell k exerts a force $\mathbf{f}_k^x + \mathbf{f}_k^y$ in both the x and y directions on the center of the active particle that is proportional to the resource level $S_g^k(t)$ at that cell and independent of the distance from the cell center to the particle center. The sign of each force component is determined by the position of the center of the cell relative to the particle center, and is positive for cells whose centers are above or to the right of the particle center, and negative for cells whose centers are below or to the left of the particle center. The total driving force on the particle is $\mathbf{F}^g = \sum_{k=1}^{12} (\mathbf{f}_k^x + \mathbf{f}_k^y)$. If the resource concentration gradient is flat along one direction, the forces exerted by the cells cancel in that direction. The theoretical maximum value of \mathbf{F}_i^g for a situation in which all of the cells on one side of the particle center have a full resource level of $S_g^k = 1$ and the remaining cells on the other side of the particle center are entirely depleted with $S_g^k = 0$ is $|\mathbf{F}_i^g| = 6$. For passive particles, $\mathbf{F}_i^g = 0$ regardless of the amount of resource present in the grid sites. Particle-particle interactions are given by a steric harmonic repulsive force, $\mathbf{F}^{pp} = \sum_{j=1}^{N_p} k(d - r_{ij})\Theta(d - r_{ij})\hat{\mathbf{r}}_{ij}$. Here $r_{ij} = |\mathbf{r}_i - \mathbf{r}_j|$, $\hat{\mathbf{r}}_{ij} = (\mathbf{r}_i - \mathbf{r}_j)/r_{ij}$, the spring constant is $k = 20.0$, Θ is the Heaviside step function, and $d = 2R$ where R is the particle radius. Integration of the equations of motion is performed with a velocity Verlet routine.

In this work we consider total particle densities $\phi = N\pi R^2/(L_x L_y)$ ranging from $\phi = 0.75$ up to $\phi = 0.935$.

For a monodisperse disk packing, the jamming density where the system forms a triangular lattice is just above $\phi = 0.91$ [28]. Thus, for densities above $\phi = 0.91$ we pass from the hard disk limit to the foam limit. The system contains N_p passive particles and N_a active particles, where $N_p + N_a = N$. The passive particles interact sterically with the active particles but have no interaction with the resource substrate.

We focus on three different regimes, shown in Fig. 2(a). In the scarce regime, with $r_{\text{abs}} = 0.0087$ and $r_{\text{rec}} = 0.000175$, the absorption rate is high and the recovery rate is low. In the balanced regime, with $r_{\text{abs}} = 0.0036$ and $r_{\text{rec}} = 0.000425$, the absorption rate is about four times higher than the recovery rate. In the plentiful regime, with $r_{\text{abs}} = 0.0009$ and $r_{\text{rec}} = 0.000825$, the absorption and recovery rates are nearly equal. For each regime, we examine in detail the behavior of the system as a function of two parameters: the density of particles and the fraction of active particles. We vary the overall particle number from $N = 4800$ to 6000 giving a density range of $0.753 < \phi < 0.942$, which spans the range from below jamming to above jamming. The fraction of passive particles N_p/N varies from 0% to 90%.

As part of our analysis, we use particle-particle contacts to define clusters of particles that are touching one another but are separated from other clusters or individual particles within the system. To compute the fraction C_L of particles in the largest cluster, we identify the sizes N_c of all of the clusters in the system by counting the number of particles in each cluster. We then use the largest value of N_c to define $C_L = N_c^{\text{max}}/N$. Additionally, we compute the time average of the absolute value of the velocities of the active, $\langle |V_a| \rangle = \langle N_a^{-1} \sum_i^{N_a} |\mathbf{v}_i| \rangle$, and passive, $\langle |V_p| \rangle = \langle N_p^{-1} \sum_i^{N_p} |\mathbf{v}_i| \rangle$, particles.

III. RESULTS

A. Scarce Regime

We first focus on the scarce regime with $r_{\text{abs}} = 0.0087$ and $r_{\text{rec}} = 0.000175$, where $r_{\text{rec}}/r_{\text{abs}} = 0.02$ and the absorption rate is about 50 times higher than the recovery rate. In Fig. 2(b) we plot a heat map of C_L , the fraction of particles that are in the largest cluster, as a function of the fraction of passive particles N_p/N versus the density ϕ . We find that strong clustering, indicated by a large value of C_L , occurs in the jammed regime at large ϕ when the fraction of passive particles is greater than $N_p/N = 0.5$. Figure 2(c) shows a heat map of $\langle |V_a| \rangle$, the average absolute value of the active particle velocities, as a function of N_p/N versus ϕ . When the fraction of passive particles is large, $\langle |V_a| \rangle$ is low, but there is a local peak in $\langle |V_a| \rangle$ near $N_p/N = 0.7$. Below this peak, $\langle |V_a| \rangle$ diminishes with decreasing N_p/N . Additionally, for $\phi > 0.89$, there is a drop in $\langle |V_a| \rangle$ associated with the onset of jamming or crystallization. In Fig. 2(d) we plot a heat map of $\langle |V_p| \rangle$, the average absolute value of the

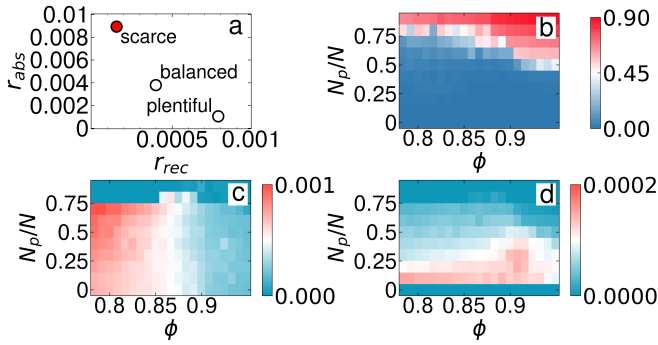


FIG. 2. (a) Illustration of the three regimes we consider as a function of absorption rate r_{abs} versus recovery rate r_{rec} : scarce with $r_{\text{abs}} = 0.0087$ and $r_{\text{rec}} = 0.000175$; balanced with $r_{\text{abs}} = 0.0036$ and $r_{\text{rec}} = 0.000425$; and plentiful with $r_{\text{abs}} = 0.0009$ and $r_{\text{rec}} = 0.000825$. (b-d) Results as a function of the fraction of passive particles N_p/N versus total density ϕ from a system in the scarce regime, marked by a red dot in panel (a). (b) Heat map of C_L , the fraction of particles in the largest cluster. (c) Heat map of $\langle |V_a| \rangle$, the average absolute value of the active particle velocities. (d) Heat map of $\langle |V_p| \rangle$, the average absolute value of the passive particle velocities.

passive particle velocities. The largest $\langle |V_p| \rangle$ appears in a band around $N_p/N = 0.1$ when there are enough active particles to push the passive particles around, but as N_p/N increases, the fraction of active particles that can perform the pushing decreases and $\langle |V_p| \rangle$ drops. There is also a drop in $\langle |V_p| \rangle$ at the highest values of ϕ where a jammed state forms consisting of a mixture of active and passive particles in a crystalline solid.

From the quantities in Fig. 2 as well as images of the system, we construct a dynamic phase diagram for the scarce regime consisting of six phases, shown in Fig. 3 as a function of N_p/N versus ϕ . In phase I, there is partial clustering of the passive particles but the velocities of both passive and active particles are low. Phase I_a , which appears only when $N_p/N > 0.75$ and $\phi > 0.9$, is a high density immobile jammed state in which the active and passive particles are intermixed into a triangular solid and the active particles are trapped by the surrounding passive particles. In phase II_a , the passive particles form a series of high density solid islands that exhibit almost no motion. Riverlike structures of active particles move between these islands through confined winding channels that slowly change over time. The channels are wide enough to permit the active particles to form a low density liquid with higher velocities $\langle |V_a| \rangle$, as shown in Fig. 2(c). In phase III_a , there is weak clustering of the passive particles, and the slowly moving active particles induce some motion of the passive particles. Within phase IV, the passive and active particles move together in a particular direction for a period of time before switching to a new collective direction of motion, forming what we call a random flocking phase in which the motion is coherent over short times but not over long

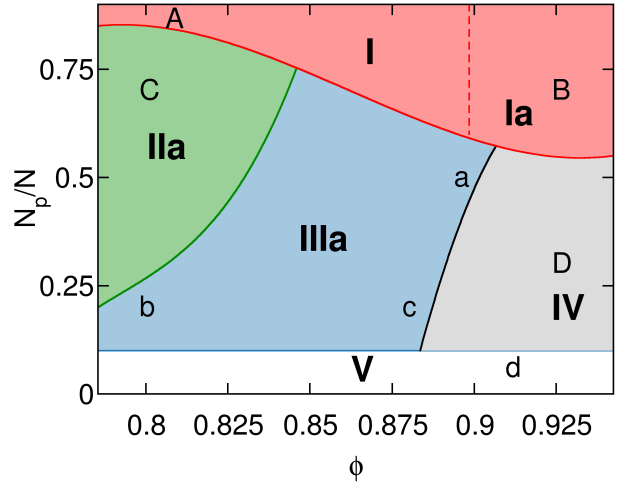


FIG. 3. Dynamic phase diagram as a function of N_p/N versus ϕ for the scarce regime with $r_{\text{abs}} = 0.0087$ and $r_{\text{rec}} = 0.000175$. The phases are: I (large passive clusters, red below dashed line), I_a (mixed jammed state, red above dashed line), II_a (rivers, green), III_a (fluctuating, blue), IV (random flocking, gray), and V (no passive particles, white). Upper case labels indicate points at which the images in Fig. 4 were obtained, while lower case labels indicate points at which the images in Fig. 5 were obtained.

times. At $N_p/N = 0$, when only active particles are present, we find phase V, which at lower densities is a liquid and for $\phi > 0.9$ is a crystalline solid that moves in a changing direction over time.

In Fig. 4 we show images from the simulations for the points marked A, B, C, and D in the phase diagram of Fig. 3. The left half of each panel shows the state of the resource substrate on a gray scale where darker color indicates greater depletion of the resource site, while the right half of each panel indicates the positions of the passive and active particles. The active particles are colored according to their velocity, where we use a cutoff velocity threshold of $|\mathbf{v}_i| < 1 \times 10^{-4}$ to indicate that an active particle is not moving or moving only very slowly. Figure 4(A) illustrates phase I at $N_p/N = 0.9$ and $\phi = 0.809$, where the velocities of both species are low. Here, the uniform background of passive particles is modulated into local clusters of passive particles with triangular ordering, and the small number of individual active particles move slowly in the regions between these clusters. As ϕ increases, the clusters of passive particles percolate, causing the cluster size C_L found in Fig. 2(b) to increase. This is correlated with the appearance of phase I_a , illustrated in Fig. 4(B) at $N_p/N = 0.7$ and $\phi = 0.927$. Phase I_a is a triangular jammed solid composed of a mixture of active and passive particles, where the triangular lattice contains a number of grain boundaries. The active particles experience gradient-induced forces from the substrate and try to move toward other sites, but because the system is so dense, this motion

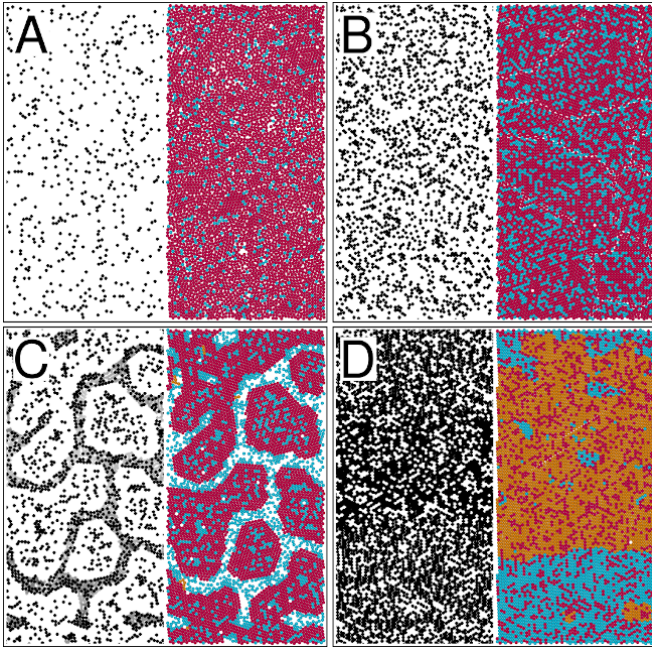


FIG. 4. Simulation images from the scarce regime with $r_{\text{abs}} = 0.0087$ and $r_{\text{rec}} = 0.000175$. The left half of each panel shows a gray scale map of the amount of resource present in the grid sites, with white indicating $S_g^i = 1$ or maximized and black indicating $S_g^i = 0$ or fully depleted. The right half of each panel shows the positions of the passive particles (red), stationary or very slowly moving active particles (orange), and active particles that are moving faster than a threshold velocity (blue). Images correspond to the points marked A, B, C, and D in the phase diagram of Fig. 3. (A) Image from point A in phase I with $N_p/N = 0.9$ and $\phi = 0.809$. (B) Image from point B in phase I_a or the jammed state with $N_p/N = 0.927$ and $\phi = 0.7$. (C) Image from point C in phase II_a at $N_p/N = 0.7$ and $\phi = 0.801$, showing riverlike ordering and flow. (D) Image from point D in phase IV_a at $N_p/N = 0.37$ and $\phi = 0.927$, where a coherently moving triangular lattice switches between different directions of motion.

is limited to the production of local compression of the lattice, which allows some lattice vacancies to form.

In Fig. 4(C) we show phase II_a at $N_p/N = 0.7$ and $\phi = 0.801$, where the active particle velocity reaches a maximum but the passive particle velocity is zero, as indicated in Fig. 2(c,d). Here the system forms a river-like state where the active particles partially segregate into low density regions of river-like paths. Along these paths, the higher concentration of active particles depletes the resource grid. The passive particles are pushed together into dense islands with local triangular ordering, but there are still some active particles trapped within these dense regions. Since the passive particles form isolated island-like structures that do not percolate, C_L does not become large in this regime. Figure 4(D) illustrates phase IV at $N_p/N = 0.37$ and $\phi = 0.927$, where we find a uniform triangular lattice in which both species are mixed. Here there are enough active particles present to cause patches of the lattice to move together in a fixed

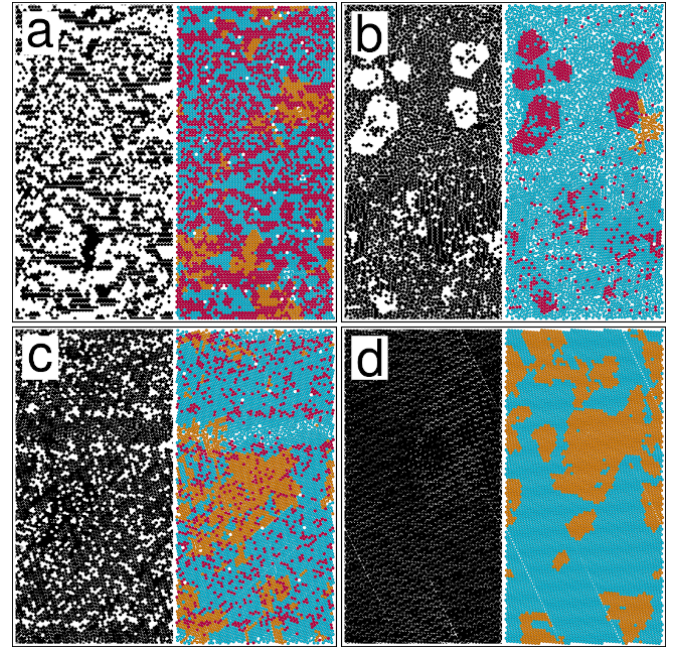


FIG. 5. Simulation images from the scarce regime with $r_{\text{abs}} = 0.0087$ and $r_{\text{rec}} = 0.000175$. The left half of each panel shows a gray scale map of the amount of resource present in the grid sites, with white indicating $S_g^i = 1$ or maximized and black indicating $S_g^i = 0$ or fully depleted. The right half of each panel shows the positions of the passive particles (red), stationary or very slowly moving active particles (orange), and active particles that are moving faster than a threshold velocity (blue). Images correspond to the points marked a, b, c, and d in the phase diagram of Fig. 3. (a) Image from point a in phase III_a at $N_p/N = 0.5$ and $\phi = 0.895$. (b) Image from point b in phase III_a at $N_p/N = 0.2$ and $\phi = 0.801$. (c) Image from point c in phase III_a at $N_p/N = 0.2$ and $\phi = 0.88$ showing increased triangular ordering. (d) Image from point d in phase V_a at $N_p/N = 0.0$ and $\phi = 0.91$, where the system forms a triangular lattice of active particles.

direction for a period of time, after which the direction of motion changes or a new patch begins to move. Since the system is so dense, the passive particles are trapped in the triangular lattice of the active particles and must move with them, producing the finite velocities of both passive and active particles found in Fig. 2(c,d).

In Fig. 5(a) we show the resource depletion and the active and passive particle positions for phase III_a at $N_p/N = 0.5$ and $\phi = 0.895$, where there is a small amount of clustering of the active particles leading to localized regions of motion. Since the system is so dense, the motion takes the form of vacancy hopping via the interchange of particles. Phase III_a is similar to the fluctuating liquid phase found at lower densities in previous work [27], but in this case there is no directed motion. Figure 5(b) shows phase III_a at $N_p/N = 0.2$ and $\phi = 0.801$, where there is a stronger tendency for the passive particles to phase separate from the active particles to form local clusters. There is, however, no large scale

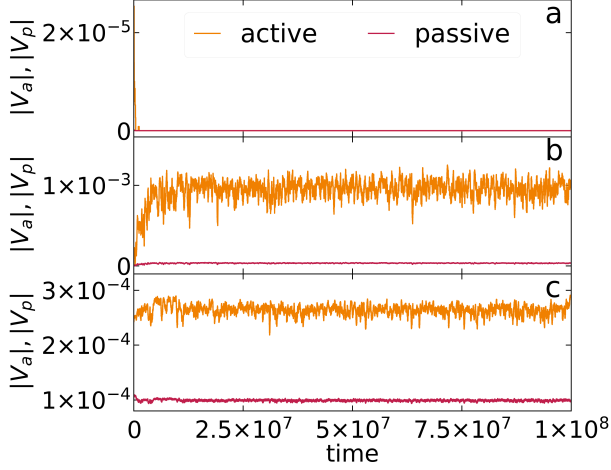


FIG. 6. Time series of $|V_a|$ (orange) and $|V_p|$ (red) in the scarce regime with $r_{\text{abs}} = 0.0087$ and $r_{\text{rec}} = 0.000175$ at labeled points from the phase diagram of Fig. 3. (a) Phase I at point A with $N_p/N = 0.9$ and $\phi = 0.809$, illustrated in Fig. 4(A), showing no motion for either type of particle. (b) Phase II_a or the river-like flow phase at point C with $N_p/N = 0.7$ and $\phi = 0.801$, illustrated in Fig. 4(C), where the active particles have a high velocity and the passive particles have a low velocity. (c) Phase IV at point D with $N_p/N = 0.37$ and $\phi = 0.927$, illustrated in Fig. 4(D), showing a higher level of motion for both the active and the passive particles.

clustering of passive particles of the type found in phases I and II_a . In Fig. 5(c), phase III_a at $N_p/N = 0.2$ and $\phi = 0.88$ has large sections of triangular ordering and the resources are more uniformly depleted. At $N_p/N = 0.0$ and $\phi = 0.91$ in phase V, shown in Fig. 5(d), the system is almost completely triangular. For lower densities, phase V becomes more fluid-like.

In Fig. 6(a) we show the time series of the absolute value of the active and passive particle velocities, $|V_a|$ and $|V_p|$, for the scarce regime with $r_{\text{abs}} = 0.0087$ and $r_{\text{rec}} = 0.000175$ in phase I from point A in the phase diagram of Fig. 3 at $N_p/N = 0.9$ and $\phi = 0.809$. Here, the velocity of both types of particle is near zero. For the phase II_a river-like flow from point C in Fig. 3 at $N_p/N = 0.7$ and $\phi = 0.801$, Fig. 6(b) shows that the active particles have a finite velocity while the velocity of the passive particles is near zero. The plot also indicates that there is a transient time during which the active particles organize the passive particles into islands, after which the system reaches a steady state. The fluctuations in $|V_p|$ in Fig. 6(b) are the result of collisions of active particles with the edges of the passive particle islands. In Fig. 6(c), the time series of $|V_a|$ and $|V_p|$ for phase IV from point D in Fig. 3 at $N_p/N = 0.37$ and $\phi = 0.927$ show that both the active and the passive particles have finite velocities, but the active particles move about 2.5 times more rapidly than the passive particles on average.

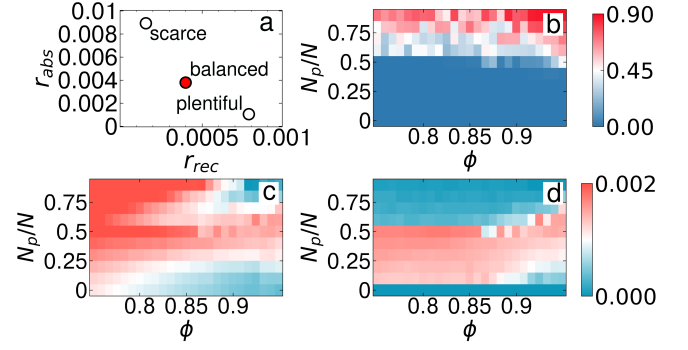


FIG. 7. (a) Diagram of the location of the scarce ($r_{\text{abs}} = 0.0087$, $r_{\text{rec}} = 0.000175$), balanced ($r_{\text{abs}} = 0.0036$, $r_{\text{rec}} = 0.000425$), and plentiful ($r_{\text{abs}} = 0.0009$, $r_{\text{rec}} = 0.000825$) regimes. (b-d) Results as a function of the fraction of passive particles N_p/N versus total density ϕ from a system in the balanced regime, marked by a red dot in panel (a), where the ratio of absorption to recovery rates is $r_{\text{abs}}/r_{\text{rec}} = 4.36$. (b) Heat map of C_L , the fraction of particles in the largest cluster. (c) Heat map of $\langle |V_a| \rangle$, the average absolute value of the active particle velocities. (d) Heat map of $\langle |V_p| \rangle$, the average absolute value of the passive particle velocities.

B. Balanced Regime

We next consider the balanced regime with $r_{\text{abs}} = 0.0036$ and $r_{\text{rec}} = 0.000825$, illustrated in Fig. 7(a), where the ratio of absorption rate to recovery rate is around 4.36. As a function of N_p/N versus ϕ , we plot heat maps of the largest cluster size C_L in Fig. 7(b), the average absolute active particle velocities $\langle |V_a| \rangle$ in Fig. 7(c), and the average absolute passive particle velocities $\langle |V_p| \rangle$ in Fig. 7(d). There is an extended window in which the velocity of both the active and the passive particles is high. For $0.754 < \phi < 0.87$ and $N_p/N > 0.4$, the active particle velocity remains high and does not drop even when $N_p/N > 0.8$, since in the fully phase separated system the active particles can move more rapidly.

Using the features in Fig. 7 along with the velocity time series and images of the particle configurations, in Fig. 8 we construct a dynamic phase diagram as a function of N_p/N versus ϕ highlighting the different phases. In general, the balanced regime exhibits extended regions of strong phase separation in which the active particles can move rapidly and shepherd the passive particles into a cluster; alternatively, the active particles themselves may undergo motility induced phase separation.

For the balanced regime, the phase separation becomes much more pronounced in phase I, and the passive particles assemble into dense clusters with triangular ordering. This is illustrated in Fig. 9(A) for phase I_b at $N_p/N = 0.8$ and $\phi = 0.801$, where the active particles herd the passive particles into crystalline stripes. In this case, the dense regions have a local density just over $\phi_{\text{loc}} = 0.91$, while in the surrounding active particle regions, the local density is well below $\phi_{\text{loc}} = 0.801$. There is no directed

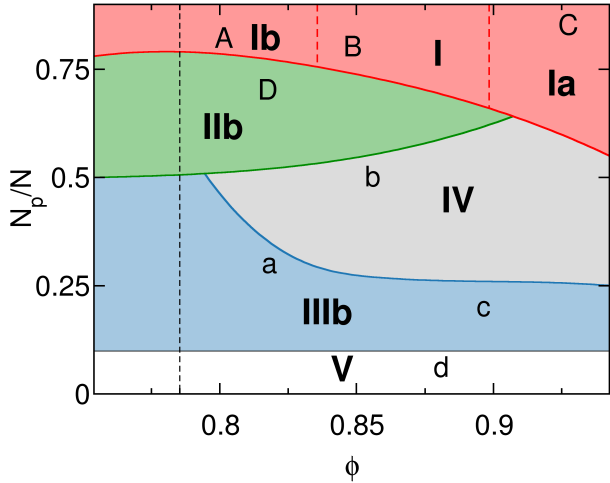


FIG. 8. Dynamic phase diagram as a function of N_p/N versus ϕ for the balanced regime with $r_{\text{abs}} = 0.0036$ and $r_{\text{rec}} = 0.000425$. The phases are: I (phase separated cluster, red center), I_a (mixed jammed state, red right), I_b (stripe-like phase separation, red left), II_b (large rivers, green), III_b (active particle clustering, blue), IV (directed motion, gray), and V (no passive particles, white).

motion of the active particles, and a small number of active particles become trapped within the passive stripes. From the heat map of $\langle |V_a| \rangle$ in Fig. 7(c), we find that the absolute value of the active particle velocities is actually higher for large N_p/N than for $N_p/N = 0$ where no passive particles are present. This seems counterintuitive since it could be thought that passive particles can only slow down the active particles; however, when the passive particles phase separate into the stripes, regions of no depletion appear underneath the stripes. As a result, a large resource gradient forms at the edge of the stripes that causes active particles along the stripe edges to move at high velocities. This can partially deform the surface of the passive stripe, and indicates that clusters or stripes of passive particles can increase the active motion in the system by facilitating the creation of large resource gradients. Figure 9(B) shows that in phase I at $N_p/N = 0.8$ and $\phi = 0.848$, due to the higher density the passive particles can form a single large connected cluster. For even higher densities we find phase I_a , as illustrated in Fig. 9(C) for $N_p/N = 0.9$ and $\phi = 0.927$. This is a uniform jammed state in which some active particles are mixed in with the passive particles. Since the strong phase separation is lost, the active particles do not experience an acceleration effect and both $\langle |V_a| \rangle$ and $\langle |V_b| \rangle$ are low.

Phase II_a from the sparse regime is replaced in the balanced regime by phase II_b , which is still a river-like phase but with much larger rivers that form large scale phase separated structures, as shown in Fig. 9(D) at $N_p/N = 0.7$ and $\phi = 0.817$. We note that the phase separated states we observe in phases I, I_a , I_c , and II_b have

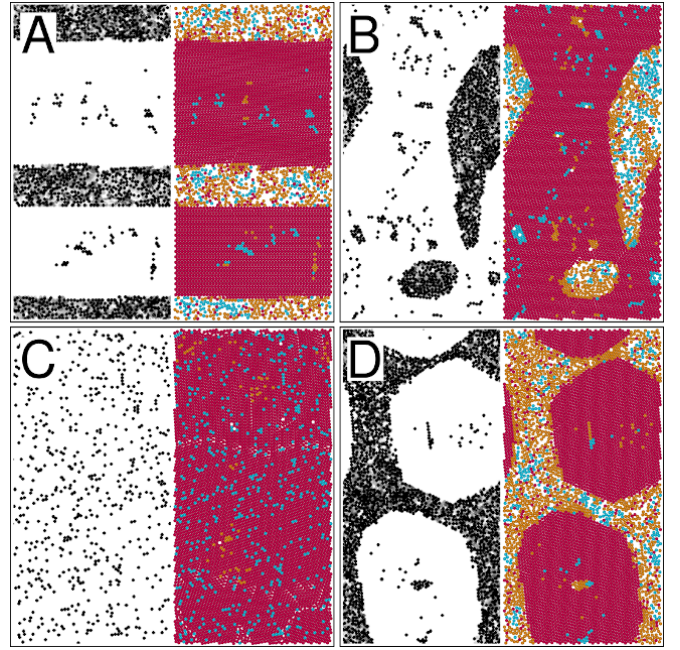


FIG. 9. Simulation images from the balanced regime with $r_{\text{abs}} = 0.0036$ and $r_{\text{rec}} = 0.000425$. The left half of each panel shows a gray scale map of the amount of resource present in the grid sites, with white indicating $S_g^i = 1$ or maximized and black indicating $S_g^i = 0$ or fully depleted. The right half of each panel shows the positions of the passive particles (red), stationary or very slowly moving active particles (orange), and active particles that are moving faster than a threshold velocity (blue). Images correspond to the points marked A, B, C, and D in the phase diagram of Fig. 8. (A) Image from point A in the low density phase I_b at $N_p/N = 0.8$ and $\phi = 0.801$. (B) Image from point B in phase I at $N_p/N = 0.8$ and $\phi = 0.848$ showing a phase separated void state. (C) Image from point C in phase I_a for $N_p/N = 0.9$ and $\phi = 0.927$ showing a jammed state with triangular ordering. (D) Image from point D in phase II_b at $N_p/N = 0.7$ and $\phi = 0.817$.

structures similar to those of phase separated states that form in equilibrium pattern forming systems with competing attractive and repulsive interactions. Such systems exhibit bubble crystals, stripes, void crystals, and uniform states as a function of increasing density [27, 30–33]. The formation of stripes or bubbles depends on the density. In general, our system forms stripes or isolated bubbles at lower passive particle densities, void-like crystals at intermediate densities, and a uniform solid at high densities. The clustering of the passive particles due to the motion of active particles over a resource substrate was also observed in Ref. [27] for much lower densities, where only isolated islands formed.

Phase III_b in Fig. 8 is also phase separated, but here the active particles form clusters while the passive particles remain in a disordered lower density liquid state, as shown in Fig. 10(a) at $N_p/N = 0.3$ and $\phi = 0.817$ and in Fig. 10(c) at $N_p/N = 0.2$ and $\phi = 0.895$. This state is similar to the motility induced phase separation found in

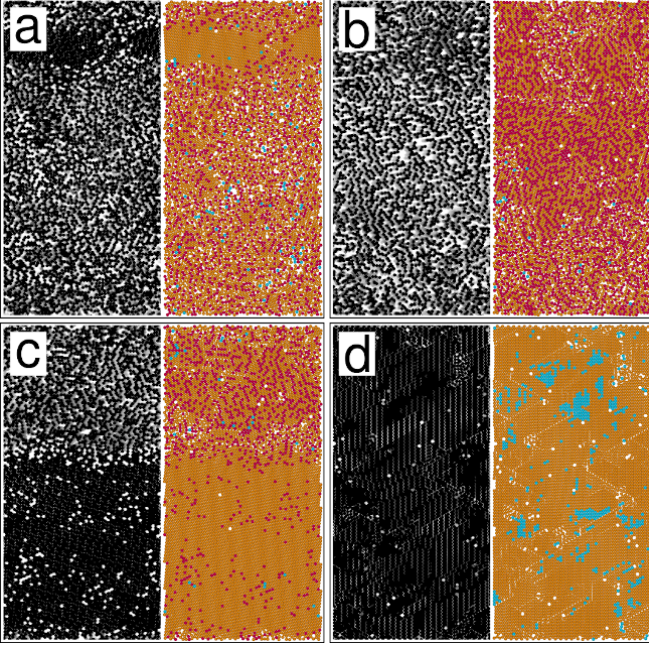


FIG. 10. Simulation images from the balanced regime with $r_{\text{abs}} = 0.0036$ and $r_{\text{rec}} = 0.000425$. The left half of each panel shows a gray scale map of the amount of resource present in the grid sites, with white indicating $S_g^i = 1$ or maximized and black indicating $S_g^i = 0$ or fully depleted. The right half of each panel shows the positions of the passive particles (red), stationary or very slowly moving active particles (orange), and active particles that are moving faster than a threshold velocity (blue). Images correspond to the points marked a, b, c, and d in the phase diagram of Fig. 8. (a) Image from point a in the active clustering phase III_b at $N_p/N = 0.3$ and $\phi = 0.817$. (b) Image from point b in phase IV at $N_p/N = 0.5$ and $\phi = 0.856$. (c) Image from point c in phase III_b at $N_p/N = 0.2$ and $\phi = 0.895$. (d) Image from point d in phase V at $N_p/N = 0$ and $\phi = 0.88$.

other active matter systems [16–21], and indicates that the motion of the active particles is now large enough to permit the active particles to form self-clustering states. In our system, phase III_b emerges when the ratio of active to passive particles is below $N_p/N = 0.5$ and when the recovery rate is high enough for the active particles to remain moving continuously. In Fig. 10(a) at $N_p/N = 0.3$ and $\phi = 0.817$, an active particle cluster with triangular ordering appears in the upper half the panel. Underneath this cluster, the resources are more strongly depleted, as indicated by the resource gray scale panel. In Fig. 10(c) at $N_p/N = 0.2$ and $\phi = 0.895$, the active cluster is much larger and the region under the active cluster shows very strong resource depletion. The size of the active cluster grows with decreasing N_p/N and increasing ϕ .

In phase III_b we find partial directed motion or flocking where clusters of active particles move collectively in a particular direction either for a period of time or, at higher densities, permanently. To illustrate this, in Fig. 11(a) we plot time series of the active particle velocities in the x and y directions, $V_a^x = N_a^{-1} \sum_i^{N_a} \mathbf{v}_i \cdot \hat{\mathbf{x}}$ and $V_a^y = N_a^{-1} \sum_i^{N_a} \mathbf{v}_i \cdot \hat{\mathbf{y}}$, respectively, for phase III_b from Fig. 8 at $N_p/N = 0.3$ and $\phi = 0.817$. There are windows of time during which the active particles move in a particular direction as a coherent flock before the motion switches into a new direction. In this case, particles in the less dense regions move faster than the particles in the dense regions. The dense region resembles what is found in traditional motility induced phase separation since the particles within this region are moving in different directions and collide with one another, leading to a reduced velocity. In the less dense region, the passive particles are entrained by the active particles and have nearly the same velocity as the active particles, as shown in Fig. 11(b) where we plot $V_p^x = N_p^{-1} \sum_i^{N_p} \mathbf{v}_i \cdot \hat{\mathbf{x}}$ and $V_p^y = N_p^{-1} \sum_i^{N_p} \mathbf{v}_i \cdot \hat{\mathbf{y}}$ for the passive particles. At higher densities, there is a change in phase III_b from directed motion in different directions to a flocking state in which all of the particles flow permanently in a fixed direction, as shown by the time series of V_a^x and V_a^y in

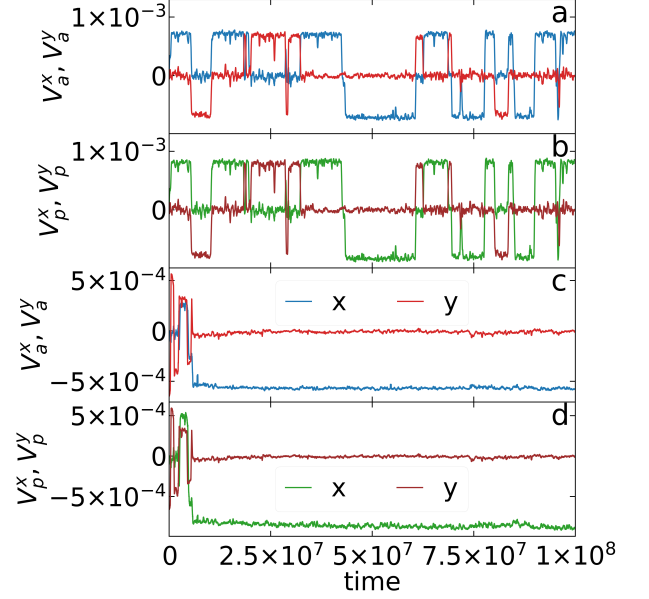


FIG. 11. Time series of the active particle velocities in the x , V_a^x (blue), and y , V_a^y (red), directions and of the passive particle velocities in the x , V_p^x (green), and y , V_p^y (maroon), directions in the balanced regime with $r_{\text{abs}} = 0.0036$ and $r_{\text{rec}} = 0.000425$ at labeled points from the phase diagram of Fig. 8. (a) V_a^x and V_a^y for phase III_b at point a with $N_p/N = 0.3$ and $\phi = 0.817$, illustrated in Fig. 10(a), where there is switching directed motion. (b) The corresponding V_p^x and V_p^y also show switching directed motion, indicating that the active particles have entrained the passive particles. (c) V_a^x and V_a^y in phase III_b from point c with $N_p/N = 0.2$ and $\phi = 0.895$, illustrated in Fig. 10(c). (d) The corresponding V_p^x and V_p^y . Here, the system settles into a state with directed motion of both particle species in the negative x direction.

ities in the x and y directions, $V_a^x = N_a^{-1} \sum_i^{N_a} \mathbf{v}_i \cdot \hat{\mathbf{x}}$ and $V_a^y = N_a^{-1} \sum_i^{N_a} \mathbf{v}_i \cdot \hat{\mathbf{y}}$, respectively, for phase III_b from Fig. 8 at $N_p/N = 0.3$ and $\phi = 0.817$. There are windows of time during which the active particles move in a particular direction as a coherent flock before the motion switches into a new direction. In this case, particles in the less dense regions move faster than the particles in the dense regions. The dense region resembles what is found in traditional motility induced phase separation since the particles within this region are moving in different directions and collide with one another, leading to a reduced velocity. In the less dense region, the passive particles are entrained by the active particles and have nearly the same velocity as the active particles, as shown in Fig. 11(b) where we plot $V_p^x = N_p^{-1} \sum_i^{N_p} \mathbf{v}_i \cdot \hat{\mathbf{x}}$ and $V_p^y = N_p^{-1} \sum_i^{N_p} \mathbf{v}_i \cdot \hat{\mathbf{y}}$ for the passive particles. At higher densities, there is a change in phase III_b from directed motion in different directions to a flocking state in which all of the particles flow permanently in a fixed direction, as shown by the time series of V_a^x and V_a^y in

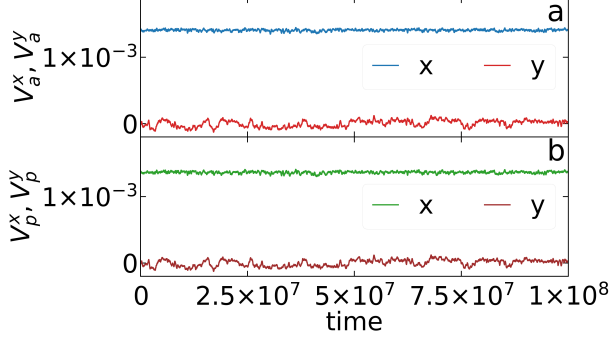


FIG. 12. (a) Time series of V_a^x (blue) and V_a^y (red) for the active particles in the balanced regime with $r_{\text{abs}} = 0.0036$ and $r_{\text{rec}} = 0.000425$ in phase IV from point b of the phase diagram in Fig. 8 with $N_p/N = 0.5$ and $\phi = 0.856$, illustrated in Fig. 10(b), showing switching directed motion. (b) The corresponding time series of V_p^x (blue) and V_p^y (maroon) for the passive particles.

Fig. 11(c) and of V_p^x and V_p^y in Fig. 11(c) for a sample with $N_p/N = 0.2$ and $\phi = 0.895$. Here, both the passive and active particles move in the negative x direction after a short transient time.

Figure 10(b) illustrates phase IV at $N/N_p = 0.5$ and $\phi = 0.856$, where the active and passive particles form a mixed cluster that depletes the resources in a more uniform manner, as indicated by the resource gray scale panel. This is a directed flocking phase in which all of the particles move in the same direction, as shown in the time series plots of V_a^x , V_a^y , V_p^x , and V_p^y in Fig. 12(a,b). Here the system settles into a state with all particles moving in the positive x direction. Additionally, the velocities of the active and passive particles are almost the same, and the system moves as a rigid body. Figure 10(d) shows an image of phase V at $N_p/N = 0$ and $\phi = 0.88$, where there are only active particles and a mostly triangular lattice forms. In this case, there is some initial directed flocking motion, but the system settles into a fluctuating state that does not exhibit directed motion. In general, it is necessary to introduce a finite fraction of passive particles in order to create sufficiently large resource gradients to induce directed motion flocking states. Resources can build up underneath the passive particles, and can then be consumed by active particles that displace the passive particles. Once the flocking motion initiates, it becomes self sustained since the moving passive particles provide fresh patches of undepleted resources that attract the active particles through the resource gradient. In turn, the active particles push the passive particles onto new sites which become the next set of resource rich locations. When the density is high enough, this directed motion can become locked to a single direction. At lower densities, local density fluctuations can break up the flock, which then reorganizes and moves in a new direction for a period of time before breaking up again. When only

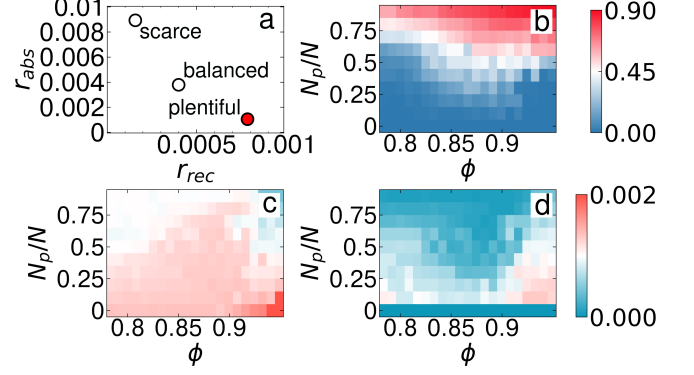


FIG. 13. (a) Diagram of the location of the scarce ($r_{\text{abs}} = 0.0087$, $r_{\text{rec}} = 0.000175$), balanced ($r_{\text{abs}} = 0.0036$, $r_{\text{rec}} = 0.000425$), and plentiful ($r_{\text{abs}} = 0.0009$, $r_{\text{rec}} = 0.000825$) regimes. (b-d) Results as a function of the fraction of passive particles N_p/N versus total density ϕ from a system in the plentiful regime, marked by a red dot in panel (a), where the ratio of absorption to recovery rates is 1.09. (b) Heat map of C_L , the fraction of particles in the largest cluster. (c) Heat map of $\langle |V_a| \rangle$, the average absolute value of the active particle velocities. (d) Heat map of $\langle |V_p| \rangle$, the average absolute value of the passive particle velocities.

active particles are present with no passive particles, the substrate depletion at this resource recovery rate is much more uniform and flocking motion does not occur.

In the balanced regime, within the intermittent flocking state at higher densities and lower passive particle fractions, we often find that the passive particles have a higher velocity than the active particles. This is because the clusters into which the active particles self-assemble often have zero net velocity. As an example, consider a system containing 100 particles, of which 70 are active and 30 are passive. If 40 of the active particles form a cluster with zero net velocity while the remaining 30 active particles are pushing around the passive particles, and if the pushed and pushing particles all have the same velocity v , then the average velocity of the active particles is $V_a = (40 \cdot 0 + 30 \cdot v)/70 \approx 0.43v$, while the average velocity of the passive particles is $V_p = (30 \cdot v)/30 = v$. Thus on average $V_p > V_a$. When the passive particle fraction is increased, the situation is reversed and the active particles have a higher average velocity than the passive particles. In our system there is generally some mixing, so that even in the regime of large N_p/N , some of the active particles are moving. As a result, we find that V_p never becomes more than 10% higher than V_a . In the scarce regime considered earlier, the active particles are not mobile enough to produce self-induced clusters, so we always find $V_a \geq V_p$.

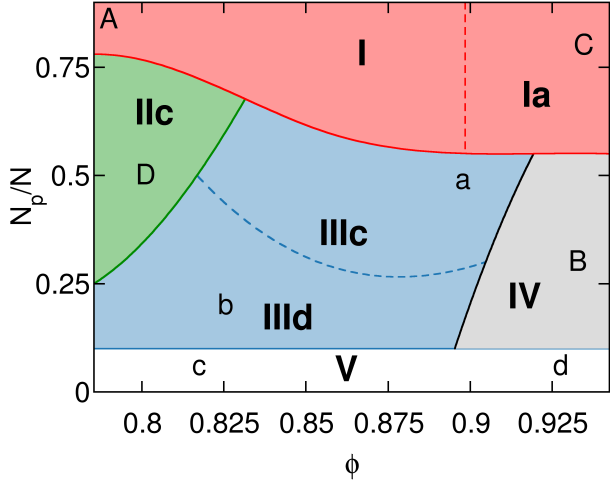


FIG. 14. Dynamic phase diagram as a function of N_p/N versus ϕ for the plentiful regime with $r_{\text{abs}} = 0.0009$ and $r_{\text{rec}} = 0.000825$. The phases are: I (phase separated cluster, red left), I_a (mixed jammed state, red right), III_c (flocking active cluster and passive solid, blue top), III_d (flocking active cluster and fluid passive mixture, blue bottom), II_c (clustering with no directed motion, green), IV (directed motion, gray), and V_a (no passive particles and directed motion, white).

IV. PLENTIFUL REGIME

In Fig. 13(b,c,d) we plot heat maps of C_L , $\langle |V_a| \rangle$, and $\langle |V_p| \rangle$ as a function of N_p/N versus ϕ in the plentiful regime with $r_{\text{abs}} = 0.0009$ and $r_{\text{rec}} = 0.000825$, indicated by the red dot in Fig. 13(a). When the recovery rate is nearly equal to the absorption rate, we find larger windows in which flocking in a fixed direction occurs. Figure 13(c) indicates that the average active particle velocity remains finite even when $N_p/N = 0$. In particular, the system with no passive particles now shows flocking behavior, so we name this state phase V_a . Phase IV still represents directed motion in which the system acts like a rigid solid moving in a single direction.

In Fig. 14 we show the dynamic phase diagram for the plentiful regime as a function of N_p/N versus ϕ . Phase I is the same phase separated cluster regime already described in which the active particles cause the passive particles to form dense clusters, while phase I_a is the same higher density mixed jammed state also found in the balanced regime. Phase III_c is similar to phase III_b in that the active particles form clusters, but now the active clusters show a flocking behavior with motion that is locked to a single direction, while the passive particles form a phase separated solid that has a lower velocity. In phase III_d , flocking active clusters still appear but the rest of the system is filled with a liquid mixture of passive and active particles. Phase II_c contains clusters of particles that undergo no directed motion. In Phase IV, we find the same mixed solid phase with directed motion as in the scarce and balanced regimes, and phase V_a con-

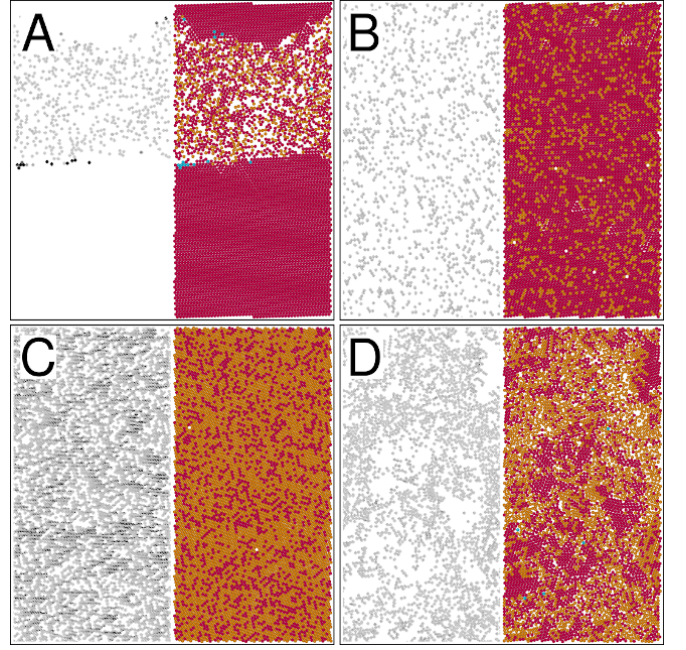


FIG. 15. Simulation images from the plentiful regime with $r_{\text{abs}} = 0.0009$ and $r_{\text{rec}} = 0.000825$. The left half of each panel shows a gray scale map of the amount of resource present in the grid sites, with white indicating $S_g^i = 1$ or maximized and black indicating $S_g^i = 0$ or fully depleted. The right half of each panel shows the positions of the passive particles (red), stationary or very slowly moving active particles (orange), and active particles that are moving faster than a threshold velocity (blue). Images correspond to the points marked A, B, C, and D in the phase diagram of Fig. 14. (A) Image from point A in phase I at $N_p/N = 0.9$ and $\phi = 0.785$, showing a strongly phase separated state. (B) Image from point B in phase IV at $N_p/N = 0.3$ and $\phi = 0.935$, where the system is in a flocking state. (C) Image from point C in phase I_a at $N_p/N = 0.8$ and $\phi = 0.935$. (d) Image from point D in phase II_c at $N_p/N = 0.8$ and $\phi = 0.801$, where the system forms a liquid state.

tains only active particles that are undergoing flocking motion.

An illustration of phase I at $N_p/N = 0.9$ and $\phi = 0.785$ appears in Fig. 15(A). The active particles are confined to lower density areas of the sample and form a fluctuating fluid containing a mixture of some passive particles. Even though the number of active particles is small, the resource is so plentiful that the active particles are very mobile and are able to push the passive particles into a single cluster. The shepherding of passive particles by active particles was previously studied in a heterogeneous system, where it was shown that when the activity of the active particles is sufficiently high, there can be an almost complete phase separation of the active and passive particles [34]. Other theoretical [35] and experimental studies [36, 37] have shown how active matter particles can assist the crystallization of passive particles. In these studies, the rapidly moving active particles did not be-

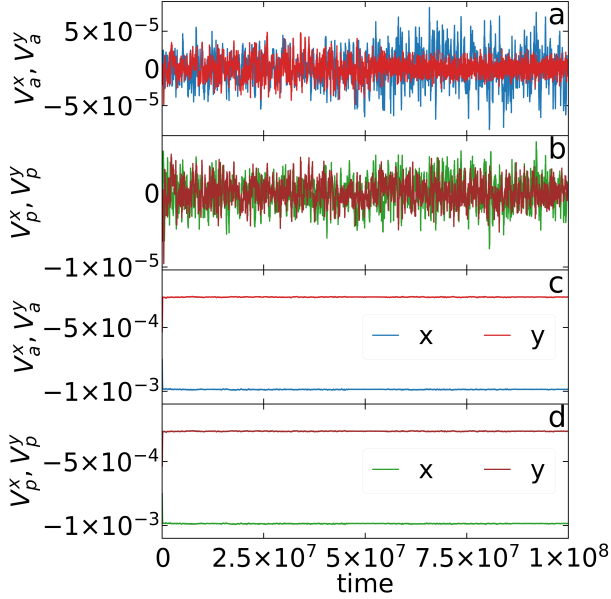


FIG. 16. Time series of the active particle velocities V_a^x (blue) and V_a^y (red) and the passive particle velocities V_p^x (green) and V_p^y (maroon) in the plentiful regime with $r_{\text{abs}} = 0.0009$ and $r_{\text{rec}} = 0.000825$ at labeled points from the phase diagram of Fig. 14. (a) V_a^x and V_a^y in phase I at point A with $N_p/N = 0.9$ and $\phi = 0.785$, illustrated in Fig. 15(A). (b) The corresponding V_p^x and V_p^y . In this case there is no directed motion. (c) V_a^x and V_a^y in phase IV from point B with $N_p/N = 0.3$ and $\phi = 0.935$, illustrated in Fig. 15(B). (d) The corresponding V_p^x and V_p^y . Here there is directed motion with both species moving in the same direction.

come trapped inside the passive clusters, unlike what we observe in the scarce and balanced regimes. In phase I_a, shown in Fig. 15(C) at $N_p/N = 0.8$ and $\phi = 0.935$, the active and passive particles are mixed and form a uniform jammed triangular solid where there is little motion. Figure 15(B) illustrates phase IV at $N_p/N = 0.3$ and $\phi = 0.935$. A uniform solid appears and moves in a flocking fashion along the x direction. Phase II_c at $N_p/N = 0.8$ and $\phi = 0.801$, shown in Fig. 15(D), has some localized clustering of passive particles, but the active particles are moving rapidly enough to break up the passive clusters and there is no coordinated directed motion. There is, however, directed motion of the clusters over short times, with each cluster moving in a particular direction for a brief period of time before rearranging and moving in a new direction for another brief period of time.

In Fig. 16(a,b) we plot time series of the velocities V_a^x , V_a^y and V_p^x , V_p^y for the active and passive particles, respectively, for phase I from Fig. 15(A). The velocities are fluctuating around zero, and although the active particles show much stronger velocity fluctuations than the passive particles, no flocking motion occurs. In phase IV from Fig. 15(B), the time series plots of V_a^x , V_a^y , V_p^x , and

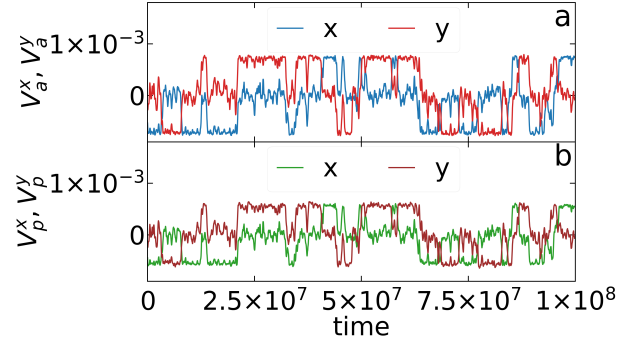


FIG. 17. (a) Time series V_a^x (blue) and V_a^y (red) for the active particles in the plentiful regime with $r_{\text{abs}} = 0.0009$ and $r_{\text{rec}} = 0.000825$ for phase II_c at point D in the phase diagram of Fig. 14 with $N_p/N = 0.8$ and $\phi = 0.801$, illustrated in Fig. 15(D), showing switching directed motion. (b) The corresponding time series V_p^x (blue) and V_p^y (maroon) for the passive particles showing that they are being fully entrained by the active particles.

V_p^y in Fig. 16(c,d) indicate that both species are moving as a solid at the same velocity. In this case, the particles are moving in the negative x and negative y directions, giving flow along an angle of -105° from the x direction. In general, the flocks can organize to move in any direction, similar to the Vicsek flocking models [23, 24].

Figure 17(a,b) shows time series of V_a^x , V_a^y , V_p^x , and V_p^y in phase II_c from Fig. 15(D). Here there is intermittent flocking of mixtures of both passive and active particles, where the direction of motion of the flocks makes abrupt changes from time to time.

In phase III_c, there is a phase separation into passive and active crystalline states where the active particles exhibit directed motion and the passive particles form an ordered crystal state at higher densities, as shown in Fig. 18(a) for $N_p/N = 0.5$ and $\phi = 0.895$. Phase III_d is an active crystal state containing liquid like passive particles, illustrated in Fig. 18(b) for $N_p/N = 0.2$ and $\phi = 0.825$. The velocity difference between the two species is higher in phase III_c than in phase III_d since the passive solid can decouple from the active solid more effectively than the passive liquid can.

In Fig. 19(a,b) we plot time series of the active and passive velocities V_a^x , V_a^y , V_p^x , and V_p^y for phase III_c from Fig. 18(a). Over time the system organizes to a state where the active particles are moving with a large velocity in the x direction while the passive particles are barely moving and have only a small velocity along the x direction due to the entrainment of some of the passive particles by the active particles. Fig. 19(c,d) shows similar velocity time series for phase III_b from Fig. 18(b). Here V_a^y is finite and V_a^x is close to zero since the active particles have organized into motion along the positive y -direction. The passive particles are also moving on average in the positive y direction but have a lower ve-

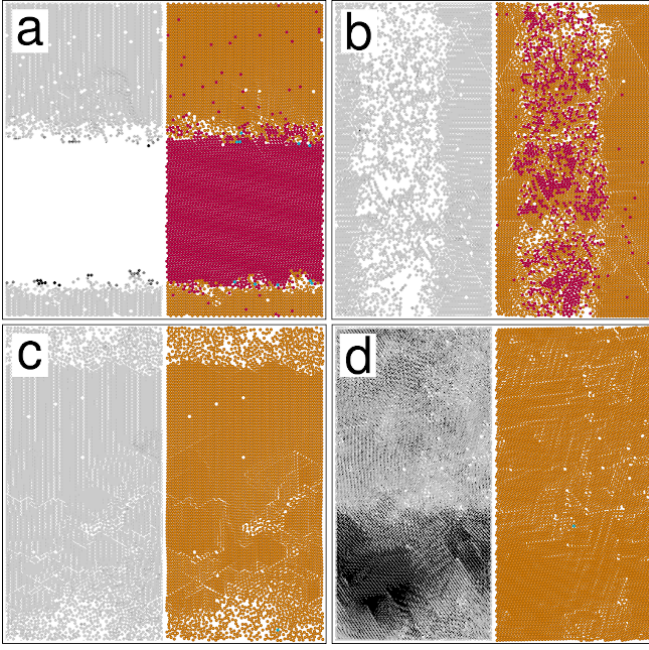


FIG. 18. Simulation images from the plentiful regime with $r_{\text{abs}} = 0.0009$ and $r_{\text{rec}} = 0.000825$. The left half of each panel shows a gray scale map of the amount of resource present in the grid sites, with white indicating $S_g^i = 1$ or maximized and black indicating $S_g^i = 0$ or fully depleted. The right half of each panel shows the positions of the passive particles (red), stationary or very slowly moving active particles (orange), and active particles that are moving faster than a threshold velocity (blue). Images correspond to the points marked a, b, c, and d in the phase diagram of Fig. 15. (a) Image from point a in phase III_c at $N_p/N = 0.5$ and $\phi = 0.895$. (b) Image from point b in phase III_d at $N_p/N = 0.2$ and $\phi = 0.825$. (c) Image from point c in phase V_a at $N_p/N = 0$ and $\phi = 0.812$. (d) Image from point d in phase V_a at $N_p/N = 0$ and $\phi = 0.927$.

locity than the active particles, since some of the passive particles are intermixed with the active cluster and are dragged along by it.

An illustration of phase V_a at $N_p/N = 0$ and $\phi = 0.812$ appears in Fig. 18(c). There is a large active cluster with triangular ordering surrounded by a lower density fluid, and the system exhibits directed motion as indicated by the time series plots of V_a^x and V_a^y in Fig. 20(a). Figure 18(d) shows phase V_a for $N_p/N = 0$ at a higher density of $\phi = 0.927$, where a mostly crystalline jammed solid moves at an angle to the y direction. The gradient in the resource substrate is clearly visible in the gray scale panel of Fig. 18(d). The active particle velocities V_a^x and V_a^y for the system in Fig. 18(d) with $\phi = 0.927$ appear in Fig. 20(b), where it is clear that the particles are moving at an angle to both the x and y directions. The flocking phases generally appear only above a critical particle density and a critical resource recovery rate. At high densities, the system generally can reach flocking configuration rather rapidly, but as the density is reduced, the period of fluctuating motion that precedes the emergence

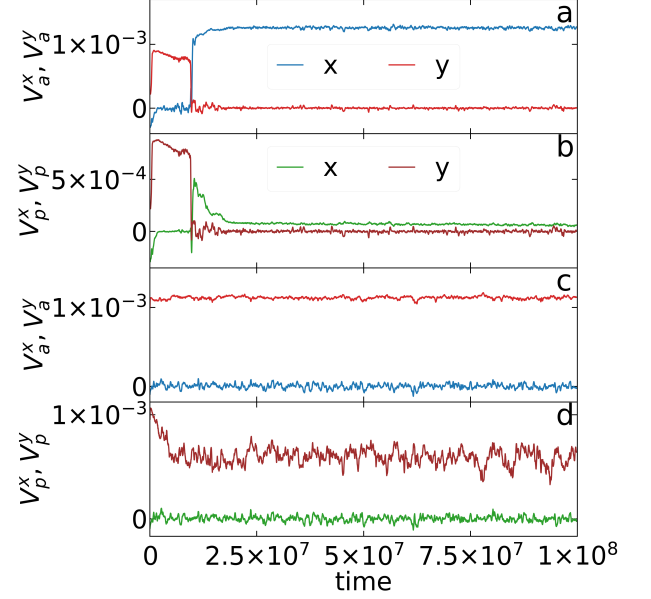


FIG. 19. Time series V_a^x (blue) and V_a^y (red) for the active particles and V_p^x (green) and V_p^y (maroon) for the passive particles in the plentiful regime with $r_{\text{abs}} = 0.0009$ and $r_{\text{rec}} = 0.000825$ at labeled points from the phase diagram of Fig. 14. (a) V_a^x and V_a^y in phase III_c at point a with $N_p/N = 0.5$ and $\phi = 0.895$, illustrated in Fig. 18(a). (b) The corresponding V_p^x and V_p^y . In this phase, the active particles are flocking but the passive particles show almost no directed motion. (c) V_a^x and V_a^y in phase III_d from point b at $N_p/N = 0.2$ and $\phi = 0.825$, illustrated in Fig. 18(b). (d) The corresponding V_p^x and V_p^y for the passive particles. In this phase, the active particles are flocking and the passive particles show limited directed motion.

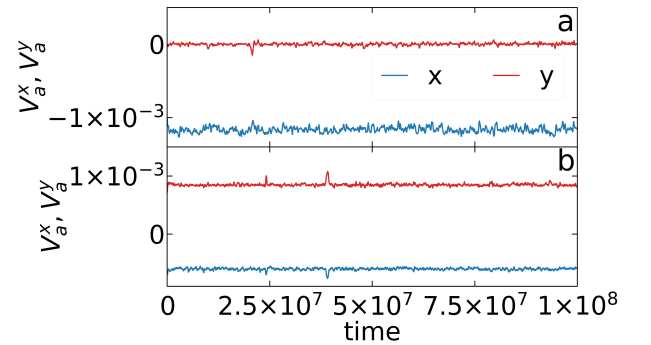


FIG. 20. Time series V_a^x (blue) and V_a^y (red) for the active particles in the plentiful regime with $r_{\text{abs}} = 0.0009$ and $r_{\text{rec}} = 0.000825$ in phase V_a from the labeled points in the phase diagram of Fig. 14 for $N_p/N = 0$, where passive particles are absent. (a) Point c with $\phi = 0.812$, illustrated in Fig. 18(c), showing flocking. (b) Point d with $\phi = 0.927$, illustrated in Fig. 18(d), also showing flocking.

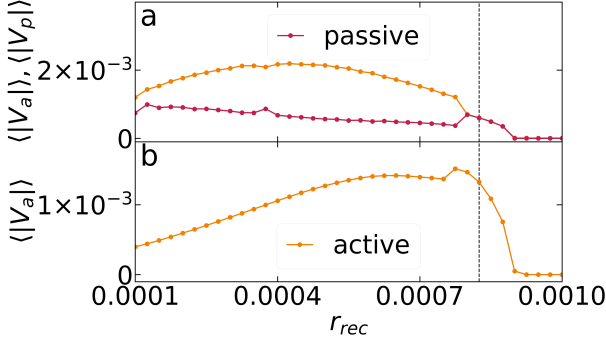


FIG. 21. (a) Average absolute value $\langle |V_a| \rangle$ (orange) of the active particles and $\langle |V_p| \rangle$ (red) of the passive particles vs r_{rec} for a sample with $\phi = 0.935$, $r_{\text{abs}} = 0.0009$, and $N_p/N = 0.8$. The dashed line corresponds to the value of r_{rec} at point C of the phase diagram in Fig. 14, where the system is phase I_a . There is a transition from phase I_a to phase III_c at $r_{\text{rec}} = 0.0008$. (b) $\langle |V_a| \rangle$ vs r_{rec} for a sample with $r_{\text{abs}} = 0.0009$, $\phi = 0.817$ and $N_p/N = 0.0$, where only active particles are present and flocking behavior appears. The dashed line corresponds to point c from the phase diagram in Fig. 14, where the system is in phase V_a . The cusp just below $r_{\text{rec}} = 0.0008$ falls at the transition from flocking in changing directions for lower r_{rec} to flocking in a fixed direction for higher r_{rec} .

of a flocking state becomes longer and longer.

We can also examine the evolution of the flocking phase by fixing the density and varying the recovery rate. In Fig. 21(a) we plot the average absolute value $\langle |V_a| \rangle$ and $\langle |V_p| \rangle$ of the active and passive particles versus r_{rec} for a system with $\phi = 0.935$, $r_{\text{abs}} = 0.0009$, and $N_p/N = 0.8$. The dashed line corresponds to point C in the phase diagram of Fig. 14, where the system is in the jammed low velocity mixed solid phase I_a , which is stable over the range $0.0008 < r_{\text{rec}} < 0.0009$. For $r_{\text{rec}} > 0.0009$, the velocity of both passive and active particles drops nearly to zero since the resources recover rapidly enough that the active particles can continuously consume resources from the grid sites without building up a resource gradient. For $0.00015 < r_{\text{rec}} < 0.0008$, the active particles form a flocking solid that is phase separated from the passive particles, so the behavior is similar to that found in phase III_c . When $r_{\text{rec}} < 0.00015$, resource depletion becomes an issue and the motion becomes pulse-like. Here the flocking is lost and the behavior resembles that of phase II_c . Overall, the flocking produces a nonmonotonic $\langle |V_a| \rangle$, indicating that there is an optimal recovery rate at which the largest flocking velocities occur. This is due to a competition between excessive resource depletion for smaller r_{rec} and disappearance of the resource gradient for larger r_{rec} . Across the III_c to I_a transition, the velocity of the active particles drops but that of the passive particles increases as the motion of the two species becomes locked together. It is beyond the scope of this work to determine whether the change from phase III_c to

phase I_a is a true phase transition; however, this would be an interesting future direction to explore.

In Fig. 21(b) we plot $\langle |V_a| \rangle$ versus r_{rec} for a system with $r_{\text{abs}} = 0.0009$, $\phi = 0.817$, and $N_p/N = 0.0$, where only active particles are present. The dashed line corresponds to point c in the phase diagram of Fig. 14 where, as shown in Fig. 18(c), the system forms a crystalline solid coexisting with a lower density fluid. A flocking solid appears for $0.00075 < r_{\text{rec}} < 0.0009$. For $r_{\text{rec}} > 0.0009$, motion ceases when the resource recovery becomes so rapid that resource gradients never form. For $r_{\text{rec}} < 0.00075$, the flocking is no longer directed but becomes intermittent, and the flocking direction changes repeatedly with relatively brief time periods spent flocking in any one direction. As the recovery rate decreases further, the switching between flocking directions becomes more frequent and the system eventually enters the pulse like flow regime studied previously [27]. Earlier work on flocking models also showed that there can be an optimal amount of disorder that produces the greatest amount of collective motion [38].

We also more closely explored the transition from flocking in repeatedly changing directions to flocking in a single direction. In Fig. 22(a,b) we plot time series of V_a^x , V_a^y , V_p^x , and V_p^y for a system in the plentiful regime at $N_p/N = 0.5$ and $\phi = 0.82$, on the boundary between phase II_c and phase III_c . During the first 7×10^7 simulation time steps, the system is in a flocking state that moves in some direction for a period of time before switching to a new direction for another period of time, and the active and passive particles are mixed together. After this long transient interval, the system settles into phase III_c where the active and passive particles decouple. Here the active particles are flocking along the $-x$ direction while the passive particles form a cluster or liquid state with no net translation. In general, as ϕ approaches the II_c - III_c boundary, it takes longer for the system to settle into a directed motion state, and at some critical density the system remains in the fluctuating phase II_c state indefinitely.

We measure the average time interval τ_s that the system in Fig. 22(a,b) spends moving in a given direction before switching to a new direction during the transient interval preceding the onset of III_c directed motion. In Fig. 22(c) we plot $1/\tau_s$ as a function of ϕ . As ϕ increases, $1/\tau_s$ becomes larger, suggesting that there is a critical density ϕ_c at which the switching time vanishes and the system forms a coherent flock. The data is not accurate enough to determine whether there is a power law divergence of $1/\tau_s$, but the results suggest that there is a critical density above which a directed motion flocking state appears. More accurate data or larger systems would be required to learn whether this transition falls into the continuous Vicsek class or whether this is an example of an absorbing phase transition [39–41], where the switching flocking behavior is the fluctuating state and the directed flocking motion is the absorbing state.

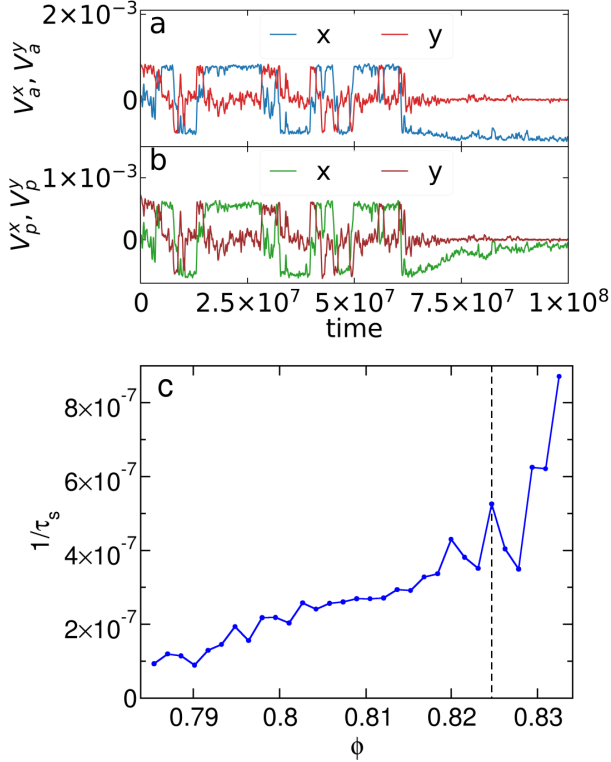


FIG. 22. (a) Time series V_a^x (blue) and V_a^y (red) for the active particles in the plentiful regime with $r_{\text{abs}} = 0.0009$ and $r_{\text{rec}} = 0.000825$ for $N_p/N = 0.5$ and $\phi = 0.82$, at the II_c to III_c transition. The system settles into a directed motion state at long times. (b) The corresponding time series of V_p^x (green) and V_p^y (maroon) for the passive particles. (c) $1/\tau_s$, the inverse of the average time interval between flocking direction switches in the transient regime of the system in panels (a) and (b), vs ϕ .

V. DISCUSSION

Our work describes a distinctive class of active matter that differs from most self-driven particle based systems, where each particle is subjected to a fixed driving force. In our system, the forces that generate the motion can vary strongly both from particle to particle and over time because they depend on the competing resource absorption and recovery processes. Despite this fact, we still observe several of the same features found in standard particle based active matter systems. For example, when the forces producing the motion of the active particles become high enough, there can be a motility induced phase separation of the active particles, or the active particles can induce a phase separation of the passive particles. In addition, our model captures features commonly observed in flocking systems, such as the formation of coherently moving states that select a symmetry-broken direction of motion. This occurs even though our model does not include an alignment term for the motion of neigh-

boring particles, which is typically required to produce flocking in Vicsek models. We also note that the directed motion we observe is different from that found in active ratchet systems [42–45], where the active particles undergo directed motion when coupled to an asymmetric substrate. In our case, the substrate is symmetric, but a dynamically generated asymmetry can arise in the resource gradient due to local density fluctuations of the active and passive particles.

Possible realizations of the model we consider include the robotic assembly on an optical resource landscape that motivated this work [25]. Our results could also be of relevance to a number of biological systems, such as crawling cells that exhibit heptotaxis by generating and then following a gradient [46–48], modifying the surface on which they are moving [49], or have their activity controlled by their rate of resource consumption [50]. There are also several models in which active particles interact with their own secreted trails [51] or undergo synthetic chemotaxis [52]. In the case of artificial swimmers, for colloids that react with a surface, the surface could regain fuel or resources over time, or the colloids could be coupled to an optical feedback that could be used to generate effective rules of motion [53, 54]. Our results could also be useful for systems near jamming [55], such as biological assemblies containing cells with different mobilities. Many other variations of this model could be explored in the future, including: adding longer range interactions; introducing spatial heterogeneity by setting certain resource sites to be always full or always empty or setting the maximum resource level of a portion of the sample to a lower level; having more than two species of particles; introducing additional types of noise; or providing rules by which active particles can transform into passive particles over time and vice versa.

VI. SUMMARY

We have introduced a model of a system of particles that move on a resource landscape grid. The system contains both active particles, which consume the resources on which they are sitting at a certain rate, and passive particles, which do not consume resources. The active particles experience a force from the substrate that is proportional to the local resource gradient, causing them to move toward sites containing higher resource levels. All particles, both active and passive, interact sterically with each other. We consider several different ratios of the resource absorption and recovery rates and also vary the particle density and the ratio of passive to active particles. Despite the simplicity of this model, we show that it exhibits a remarkable number of phases, including motility induced phase separated states, clustering of the active particles, and directed flocking motion. In the scarce regime where resource absorption is dominant, we find different types of mixed phases and riverlike phase separated flows, while at higher densities,

mixed jammed states appear. For the balanced regime where the resource absorption rate is about four times higher than the recovery rate, we observe a wealth of phase separated regimes with different morphologies, including stripe, bubble, and void states. The activity in the balanced regime is high enough that the active particles are able to self-cluster and form a motility induced phase separated state. As the fraction of passive particles increases, the mobility of the active particles can increase due to the formation of large resource gradients at the edges of the passive particle clusters. We also find a directed flocking motion regime in which the particles all move in a symmetry broken direction due to the generation of a self-sustaining resource gradient. This directed motion resembles the flocking states found in Vicsek models, and it appears in systems containing only active particles as well as for mixtures of active and passive particles at high densities where a jammed solid forms. In the plentiful regime where the absorption and recovery rates are nearly equal, we find an increased number of flocking regimes. Here the phase separation can become so strong that the active particles decouple from the passive particles. The flocking mobility varies non-monotonically with changing resource recovery rate. For the highest recovery rates, there is no motion since re-

source gradients never form, while at low recovery rates, there is only a low level of intermittent motion since sizeable gradients only slowly form. As a result, there is an optimal recovery rate for generating the greatest amount of directed mobility. In general, there is a transient period in which the flocking motion repeatedly switches directions before eventually settling down into motion in a single direction. The time interval between direction switches decreases as the density of the system increases. We discuss how our system could be relevant for various types of biological or robotic systems, colloids on reactive substrates, or colloids with optical feedback control.

ACKNOWLEDGMENTS

This work was supported by the US Department of Energy through the Los Alamos National Laboratory. Los Alamos National Laboratory is operated by Triad National Security, LLC, for the National Nuclear Security Administration of the U. S. Department of Energy (Contract No. 892333218NCA000001). LV and AL were supported by a grant of the Romanian Ministry of Education and Research, CNCS - UEFISCDI, project number PN-III-P4-ID-PCE-2020-1301, within PNCDI III.

-
- [1] S. Bhattacharya and M. J. Higgins, “Dynamics of a disordered flux line lattice,” *Phys. Rev. Lett.* **70**, 2617–2620 (1993).
 - [2] G. Blatter, M. V. Feigel’man, V. B. Geshkenbein, A. I. Larkin, and V. M. Vinokur, “Vortices in high-temperature superconductors,” *Rev. Mod. Phys.* **66**, 1125–1388 (1994).
 - [3] C. Reichhardt and C. J. Olson, “Colloidal dynamics on disordered substrates,” *Phys. Rev. Lett.* **89**, 078301 (2002).
 - [4] A. Pertsinidis and X. S. Ling, “Statics and dynamics of 2D colloidal crystals in a random pinning potential,” *Phys. Rev. Lett.* **100**, 028303 (2008).
 - [5] P. Tierno, “Depinning and collective dynamics of magnetically driven colloidal monolayers,” *Phys. Rev. Lett.* **109**, 198304 (2012).
 - [6] A. Vanossi, N. Manini, M. Urbakh, S. Zapperi, and E. Tosatti, “Colloquium: Modeling friction: From nanoscale to mesoscale,” *Rev. Mod. Phys.* **85**, 529–552 (2013).
 - [7] D. S. Fisher, “Collective transport in random media: from superconductors to earthquakes,” *Phys. Rep.* **301**, 113–150 (1998).
 - [8] C. Reichhardt and C. J. Olson Reichhardt, “Depinning and nonequilibrium dynamic phases of particle assemblies driven over random and ordered substrates: a review,” *Rep. Prog. Phys.* **80**, 026501 (2017).
 - [9] F. Pardo, F. de la Cruz, P. L. Gammel, E. Bucher, and D. J. Bishop, “Observation of smectic and moving-Bragg-glass phases in flowing vortex lattices,” *Nature* **396**, 348–350 (1998).
 - [10] C. J. Olson, C. Reichhardt, and F. Nori, “Nonequilibrium dynamic phase diagram for vortex lattices,” *Phys. Rev. Lett.* **81**, 3757–3760 (1998).
 - [11] J. Dzubiella, G. P. Hoffmann, and H. Löwen, “Lane formation in colloidal mixtures driven by an external field,” *Phys. Rev. E* **65**, 021402 (2002).
 - [12] T. Vissers, A. van Blaaderen, and A. Imhof, “Band formation in mixtures of oppositely charged colloids driven by an ac electric field,” *Phys. Rev. Lett.* **106**, 228303 (2011).
 - [13] C. Reichhardt and C. J. O. Reichhardt, “Velocity force curves, laning, and jamming for oppositely driven disk systems,” *Soft Matter* **14**, 490–498 (2018).
 - [14] M. C. Marchetti, J. F. Joanny, S. Ramaswamy, T. B. Liverpool, J. Prost, M. Rao, and R. A. Simha, “Hydrodynamics of soft active matter,” *Rev. Mod. Phys.* **85**, 1143–1189 (2013).
 - [15] C. Bechinger, R. Di Leonardo, H. Löwen, C. Reichhardt, G. Volpe, and G. Volpe, “Active particles in complex and crowded environments,” *Rev. Mod. Phys.* **88**, 045006 (2016).
 - [16] Y. Fily and M. C. Marchetti, “Athermal phase separation of self-propelled particles with no alignment,” *Phys. Rev. Lett.* **108**, 235702 (2012).
 - [17] G. S. Redner, M. F. Hagan, and A. Baskaran, “Structure and dynamics of a phase-separating active colloidal fluid,” *Phys. Rev. Lett.* **110**, 055701 (2013).
 - [18] J. Palacci, S. Sacanna, A. P. Steinberg, D. J. Pine, and P. M. Chaikin, “Living crystals of light-activated colloidal surfers,” *Science* **339**, 936–940 (2013).
 - [19] I. Buttinoni, J. Bialké, F. Kümmel, H. Löwen, C. Bechinger, and T. Speck, “Dynamical clustering and

- phase separation in suspensions of self-propelled colloidal particles,” *Phys. Rev. Lett.* **110**, 238301 (2013).
- [20] M. E. Cates and J. Tailleur, “Motility-induced phase separation,” *Annual Review of Condensed Matter Physics* **6**, 219–244 (2015).
- [21] C. Reichhardt and C. J. Olson Reichhardt, “Active microrheology in active matter systems: Mobility, intermittency, and avalanches,” *Phys. Rev. E* **91**, 032313 (2015).
- [22] Cs. Sándor, A. Libál, C. Reichhardt, and C. J. Olson Reichhardt, “Dynamic phases of active matter systems with quenched disorder,” *Phys. Rev. E* **95**, 032606 (2017).
- [23] T. Vicsek and A. Zafeiris, “Collective motion,” *Phys. Rep.* **517**, 71 (2012).
- [24] A. Morin, N. Desreumaux, J.-B. Caussin, and D. Bartolo, “Distortion and destruction of colloidal flocks in disordered environments,” *Nature Phys.* **13**, 63–67 (2017).
- [25] G. Wang, T. V. Phan, S. Li, M. Wombacher, J. Qu, Y. Peng, G. Chen, D. I. Goldman, S. A. Levin, R. H. Austin, and L. Liu, “Emergent field-driven robot swarm states,” *Phys. Rev. Lett.* **126**, 108002 (2021).
- [26] G. Wang, T. V. Phan, S. Li, J. Wang, Y. Peng, G. Chen, J. Qu, D. I. Goldman, S. A. Levin, K. Pienta, S. Amend, R. H. Austin, and L. Liu, “Robots as models of evolving systems,” *Proc. Natl. Acad. Sci. (USA)* **119**, e2120019119 (2022).
- [27] L. Varga, A. Libál, C. J. O. Reichhardt, and C. Reichhardt, “Active regimes for particles on resource landscapes,” *Phys. Rev. Research* **4**, 013061 (2022).
- [28] C. Reichhardt and C. J. Olson Reichhardt, “Aspects of jamming in two-dimensional athermal frictionless systems,” *Soft Matter* **10**, 2932–2944 (2014).
- [29] V. S. Zykov and E. Bodenschatz, “Wave propagation in inhomogeneous excitable media,” *Ann. Rev. Condens. Matter Phys.* **9**, 435 (2018).
- [30] M. Seul and D. Andelman, “Domain shapes and patterns - the phenomenology of modulated phases,” *Science* **267**, 476–483 (1995).
- [31] G. Malescio and G. Pellicane, “Stripe phases from isotropic repulsive interactions,” *Nature Mater.* **2**, 97–100 (2003).
- [32] C. J. Olson Reichhardt, C. Reichhardt, and A. R. Bishop, “Structural transitions, melting, and intermediate phases for stripe- and clump-forming systems,” *Phys. Rev. E* **82**, 041502 (2010).
- [33] J. F. Neto and C. C. de Souza Silva, “Mesoscale phase separation of skyrmion-vortex matter in chiral-magnet-superconductor heterostructures,” *Phys. Rev. Lett.* **128**, 057001 (2022).
- [34] P. Forgács, A. Libál, C. Reichhardt, and C. J. O. Reichhardt, “Active matter shepherding and clustering in inhomogeneous environments,” *Phys. Rev. E* **104**, 044613 (2021).
- [35] R. Ni, M. A. Cohen Stuart, M. Dijkstra, and P. G. Bolhuis, “Crystallizing hard-sphere glasses by doping with active particles,” *Soft Matter* **10**, 6609 (2014).
- [36] F. Kümmel, P. Shabestari, C. Lozano, G. Volpe, and C. Bechinger, “Formation, compression and surface melting of colloidal clusters by active particles,” *Soft Matter* **11**, 6187–6191 (2015).
- [37] S. Ramanananarivo, E. Ducrot, and J. Palacci, “Activity-controlled annealing of colloidal monolayers,” *Nature Commun.* **10**, 3380 (2019).
- [38] O. Chepizhko, E. G. Altmann, and F. Peruani, “Optimal noise maximizes collective motion in heterogeneous media,” *Phys. Rev. Lett.* **110**, 238101 (2013).
- [39] H. Hinrichsen, “Non-equilibrium critical phenomena and phase transitions into absorbing states,” *Adv. Phys.* **49**, 815–958 (2000).
- [40] L. Corte, P. M. Chaikin, J. P. Gollub, and D. J. Pine, “Random organization in periodically driven systems,” *Nature Phys.* **4**, 420–424 (2008).
- [41] C. Reichhardt and C. J. Olson Reichhardt, “Absorbing phase transitions and dynamic freezing in running active matter systems,” *Soft Matter* **10**, 7502–7510 (2014).
- [42] M. B. Wan, C. J. Olson Reichhardt, Z. Nussinov, and C. Reichhardt, “Rectification of swimming bacteria and self-driven particle systems by arrays of asymmetric barriers,” *Phys. Rev. Lett.* **101**, 018102 (2008).
- [43] C. J. Olson Reichhardt and C. Reichhardt, “Ratchet effects in active matter systems,” *Ann. Rev. Condens. Matter Phys.* **8**, 51–75 (2017).
- [44] A. D. Borba, Jorge L. C. Domingos, E. C. B. Moraes, F. Q. Potiguar, and W. P. Ferreira, “Controlling the transport of active matter in disordered lattices of asymmetrical obstacles,” *Phys. Rev. E* **101**, 022601 (2020).
- [45] J. O’Byrne, Y. Kafri, J. Tailleur, and F. van Wijland, “Time irreversibility in active matter, from micro to macro,” *Nature Rev. Phys.* **4**, 167–183 (2022).
- [46] M. Weber, R. Hauschild, J. Schwarz, C. Moussion, I. de Vries, D. F. Legler, S. A. Luther, T. Bollenbach, and M. Sixt, “Interstitial dendritic cell guidance by haptotactic chemokine gradients,” *Science* **339**, 328–332 (2013).
- [47] L. Tweedy, O. Susanto, and R. H. Insall, “Self-generated chemotactic gradients - cells steering themselves,” *Curr. Opin. Cell Biol.* **42**, 46–51 (2016).
- [48] E. Doná, J. D. Barry, G. Valentin, C. Quirin, A. Khmelinskii, A. Kunze, S. Durdu, L. R. Newton, A. Fernandez-Minan, W. Huber, M. Knop, and D. Gilmour, “Directional tissue migration through a self-generated chemokine gradient,” *Nature (London)* **503**, 285–289 (2013).
- [49] J. Solon, P. Streicher, R. Richter, F. Brochard-Wyart, and P. Bassereau, “Vesicles surfing on a lipid bilayer: self-induced haptotactic motion,” *Proc. Natl. Acad. Sci. (USA)* **103**, 12382 (2006).
- [50] O. Cochet-Escartin, M. Demircigil, S. Hirose, B. Allais, P. Gonzalo, I. Mikaelian, K. Funamoto, C. Anjard, V. Calvez, and J.-P. Rieu, “Hypoxia triggers collective aerotactic migration in *dictyostelium discoideum*,” *eLife* **10**, e64731 (2021).
- [51] A. Sengupta, S. van Teeffelen, and H. Löwen, “Dynamics of a microorganism moving by chemotaxis in its own secretion,” *Phys. Rev. E* **80**, 031122 (2009).
- [52] B. Liebchen and H. Löwen, “Synthetic chemotaxis and collective behavior in active matter,” *Acc. Chem. Res.* **51**, 2982–2990 (2018).
- [53] F. A. Lavergne, H. Wendehenne, T. Baeuerle, and C. Bechinger, “Group formation and cohesion of active particles with visual perception-dependent motility,” *Science* **364**, 70 (2019).
- [54] S. Yang, M. Huang, Y. Zhao, and H. P. Zhang, “Controlling cell motion and microscale flow with polarized light fields,” *Phys. Rev. Lett.* **126**, 058001 (2021).
- [55] D. Bi, X. Yang, M. C. Marchetti, and M. L. Manning, “Motility-driven glass and jamming transitions in biological tissues,” *Phys. Rev. X* **6**, 021011 (2016).